C. K. H. Koh
School of Mechanical and Production Engineering, Nanyang Technological University, Singapore

J. Shi
Industrial and Operations Engineering Department

W. J. Williams
Electrical Engineering and Computer Science Department

J. Ni
Mechanical Engineering and Applied Mechanics Department

University of Michigan, Ann Arbor, MI 48109

Multiple Fault Detection and Isolation Using the Haar Transform, Part 2: Application to the Stamping Process

The sheet metal drawing operation is a complex manufacturing process involving more than forty process variables. The intricate interaction among these variables affect the forming tonnage which is measured by strain gages mounted on the press. A fault is said to occur when any of these process variables deviate beyond their specified limits. Current detection schemes based on thresholding do not fully exploit the information in the tonnage signals for the detection and isolation of multiple fault condition. It is thus an excellent case study for demonstrating the implementation of the detection methodology presented in Part 1. By partitioning the tonnage signature into disjoint segments, mutually exclusive sets of Haar coefficients can be used to isolate faults in each stage of the process.

1 Introduction

The three-dimensional forming of sheet metal is a process which uses a pair of top and bottom die sets to shape the sheet metal into its final form under considerable pressure. Most deep drawing dies have separate outer binders to regulate the flow of material as the inner punch draws the material into the lower die. Both the forces generated by the outer blankholding binders and the inner punch have significant impact on the quality of the part produced. These forces are also highly sensitive to changes in a number of process variables [1], [4]–[5] [10] which may be broadly classified under: material properties, die set variables, press variables and interactive variables. Tonnage signatures are altered either directly by changes in these process variables or indirectly by occasions of splits, wrinkles or slugs in the drawing stage. A typical tonnage signature indicating the different features of the process is shown in Fig. 1.

Although monitoring systems for peak loads and tonnage variation as a function of time, ram position or crank angle [2], [3] are quite common, they do not incorporate any kind of fault isolation or diagnostic algorithm. They feature upper and lower control limits on the tonnage variation over the entire press cycle and automatically stop the process when these thresholds are exceeded. Fault diagnosis is seldom quantitative and depends on the experience of the technician who "eyeballs" errant signatures for some indications of the fault.

Some attempts have been made to develop some kind of diagnostic tool for the forming process based on tonnage signatures. Martinez-Heath and Bortfeld [7] used the number of threshold crossings of the control limits of the template signature to discriminate between good and bad processes. Seem and Knussman [9] used the statistical measurements of peak tonnage to detect worn dies. Both of these methods however are only effective for faults with significant amplitude changes. Faults which alter only the frequency content of the tonnage signal (for example, gib chatter) would escape detection by the amplitude-based control limits. Furthermore, both papers addressed only the detection of a specific fault and do not discuss the impact of multiple faults on their detection schemes.

This paper demonstrates how the detection methodology presented in Part 1 can be implemented as an on-line (automatic) fault detection and isolation scheme for the stamping process. The implementation of the detector is discussed in section 2 and the detector performance is evaluated in section 3. The conclusion is found in section 4.

2 Implementation of the Haar Detector

The stamping process is a good example of a manufacturing process where *a priori* information on most fault signals is seldom available. Structural faults rarely occur if the press has been properly operated and maintained. Such faults include broken pitmans, cracked uprights and loose tie-rods. When faults do occur, the press is often shut down almost immediately by the tonnage monitoring system. It will be shown that the Haar coefficients which acquire new "highs" [4] under fault condition can be successfully used as detection signals. The statistical properties of fault signals become superfluous.

Using the reasoning in section 3, Part 1, the problem can be formulated by the following hypotheses:

Case 1. No fault condition:

$$H_o : c \sim N(m_o, \sigma_o^2)$$

Case 2. Fault condition:

$$H_1 : c \sim N(m_1, \sigma_o^2)$$

where c is the observation of c_i arriving at the detector. The mean values of c_i under H_o and H_1 are denoted by m_o and m_1 respectively. It is assumed that the process noise represented by the variance σ_o^2 remains unchanged throughout.

The Haar detector is implemented as follows.

Step 1. Segmentation of Signal

Partition the tonnage signal, $\underline{X} = \{x_i\}_{i=1}^{n}$, into J disjoint segments, $\{S_j\}_{j=1}^{J}$, such that

$$\underline{X} = \bigcup_j S_j$$

Each segment S_j covers a particular stage of the forming process; and a set of faults, F_j, is associated with this process stage. The

Contributed by the Manufacturing Engineering Division for publication in the JOURNAL OF MANUFACTURING SCIENCE AND ENGINEERING. Manuscript received Oct. 1996; revised April 1998. Associate Technical Editor: M. Elbestawi.

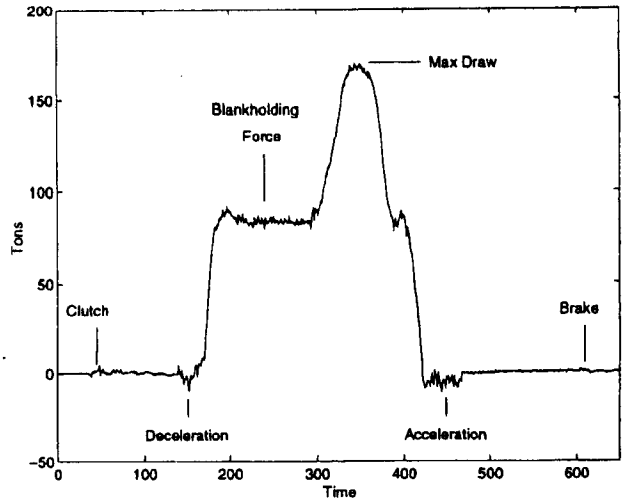

Fig. 1 Typical tonnage signature of a double-action, overdrive press

segments $\{S_j\}_{j=1}^{J}$ are partitioned according to the motion curves of the press. These segments will be referenced by the crank angle of the mainshaft. For an N-bit angle decoder, there will be $n = 2^N$ data points for each press cycle or 360 deg of crank rotation.

Step 2. Select Sets of Haar Coefficients

If $[x_1 : x_2]$ is the width of the data segment and $[k_1 : k_2]$ is the region of support for any Haar function, then a Haar function which lies within the segment S_j is bounded by the condition (10) in Part 1.

$$\{k_1 \geq x_1\} \cap \{k_2 \leq x_2\}$$

A set of such functions can be found and the corresponding Haar coefficients denoted by C_j. Consequently, J disjoint sets of Haar coefficients $\{C_j\}_{j=1}^{J}$ can be found where

$$C_k \cap C_l = 0, \quad \forall k \neq l$$

These disjoint sets of Haar coefficients allow detection of multiple faults occurring at different stages of the process during the same press cycle. A further reduction in the dimensions of C_j, $j = 1, \ldots, J$ can be achieved by sensitivity analysis (Part 1, section 2.5) if the fault signals are known in advance, or by simply neglecting higher indexed coefficients which represent the process noise.

Step 3. Establish Detection Threshold

The UMP threshold for each Haar coefficient is computed from (30) in Part 1, using data collected during normal operation of the press. The mean and standard deviation of a Haar coefficient c_i can be determined from (14) and (15) in Part 1. The value of λ is read off a table [6] when a level of significance, α, has been predetermined.

Step 4. Monitor the Sets $C_j, j = 1, 2, \ldots, J$

Apply the UMP to detect jumps in the selected Haar coefficients, that is, all $c_i \in \{C_j\}_{j=1}^{J}$. A counter is used to record the number of times a coefficient exceeds its threshold. The UMP threshold for the cumulative threshold crossing or hits for each of the Haar sets $C_j, j = 1, \ldots, J$, is also determined using the threshold (30) in Part 1. Let $\mathscr{A}_j, j = 1, \ldots, J$ be the cumulative hits for the Haar sets $C_j, j = 1, \ldots, J$ after every stroke. The mean cumulative hits under normal condition is zero (since there should not be any hit under normal condition). The standard deviation is simply estimated from the number of hits under normal conditions.

Step 5. Identify Location of the Fault

When $\mathscr{A}_j$ crosses its UMP threshold, an alarm is registered at the output of the detector for segment S_j. The use of cumulative threshold crossing (of the coefficients in C_j) has an averaging effect on the process noise. The number of false crossings due to noisy processes is thus significantly reduced.

3 Test Results

The following test results were obtained from a set of surrogate signals generated from 150 consecutive cycles of a Clearing double-action overdrive press. Surrogate signals are normal tonnage signals modified to duplicate the kind of features expected in the fault signatures. They retain the characteristics of the original process noise and are reasonably good surrogates of real fault signals.

Four types of surrogate fault signals were tested (Fig. 2). They are typical of process variables which are frequently encountered in the stamping process [8]. They are (*a*) F_1—material too thick (*b*) F_2—material too thin (*c*) F_3—loose tie rods and (*d*) F_4—worn bushings. Both (*a*) and (*b*) arise from changes in the material thickness process variable, and they are time-shifted versions of each other. They are difficult to distinguish by eye without alignment. Fault types (*c*) and (*d*) are related to process variables under machine adjustments. They have almost the same magnitudes and differ only by an additional low amplitude sinusoidal component in (*d*). It is nearly impossible to visually differentiate between (*c*) and (*d*).

1. Segmenting the Signal

Each realization is $2^N = 512$ data points long and segmented using the motion curve for the press (Fig. 3).

2. Selecting the Sets of Haar Coefficients

The disjoint sets of Haar coefficients for data segments S_1 and S_2 were determined from the condition: $\{k_1 \geq x_1\} \cap \{k_2 \leq x_2\}$. A total of 94 coefficients for C_1 and 32 for C_2 were obtained. The distribution of $\{c_i\} \in C_1, C_2$ in the original set C is indicated by the numbers on the vertical axis of Fig. 4. Higher indexed coefficients (>44 for C_1 and >14 for C_2) may be neglected as they represent mostly process noise information.

3. Establishing the Detection Threshold

The mean ($\bar{c}_i$) and standard deviation (σ_i) for each coefficient in C_1 and C_2 are estimated from the normal data using (16) and (17). An unbiased estimator is used to determine σ_i. A threshold based on $\alpha = 0.01$, and hence $\lambda = 2.3$, can be found for each $c_i \in C_1, C_2$.

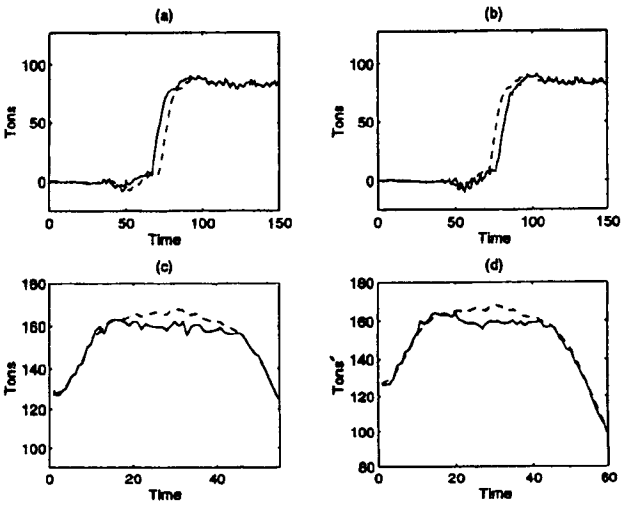

Fig. 2 Fault signals used in the test. Template signature (----) is shown superimposed on a sample of the faults (*a*) F_1—material too thick (*b*) F_2—material too thin (*c*) F_3—loose tie rod (*d*) F_4—worn bushing. Faults F_1 and F_2 are found in segment S_1 while F_3 and F_4 are found in segment S_2 in Fig. 3.

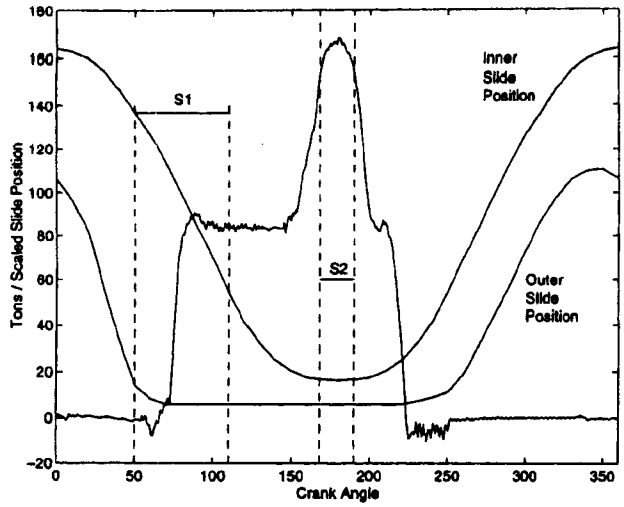

Fig. 3 Motion curves and tonnage signature. Faults F_1 and F_2 are found in data segment S_1 and faults F_3 and F_4 are found in data segment S_2.

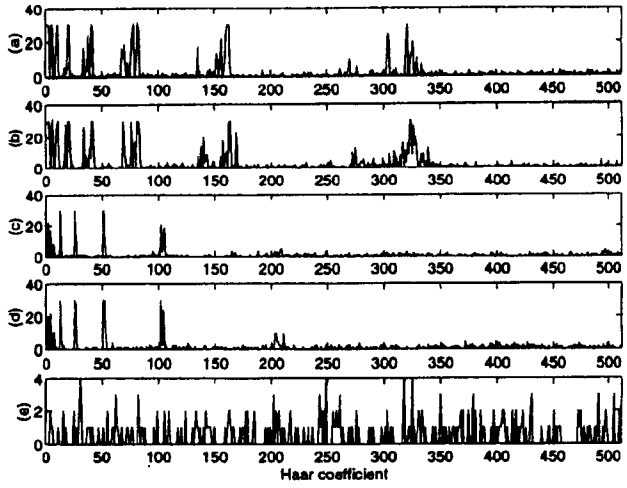

Fig. 5 Hits recorded by each of the 512 Haar coefficients for (*a*) fault F_1, (*b*) fault F_2, (*c*) fault F_3, (*d*) fault F_4, and (*e*) normal signal, based on a level of significance, $\alpha = 0.01$

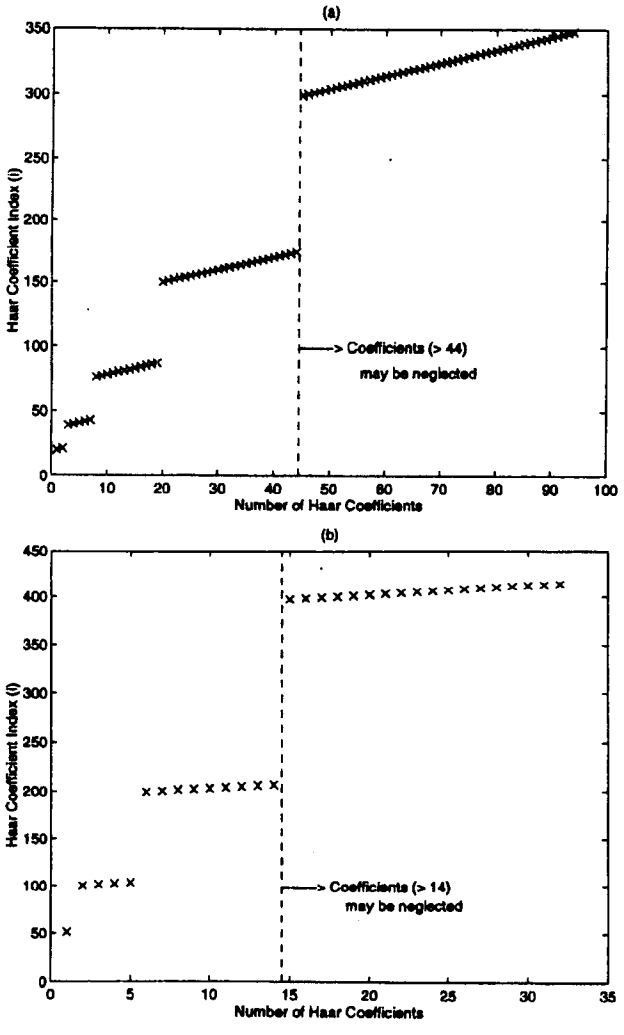

Fig. 4 Haar coefficient sets (*a*) C_1 and (*b*) C_2 for segments S_1 and S_2 respectively. The vertical axis indicate the position, $i = 2^r + m$, of the coefficient, $c\underline{C} = H\underline{X}$.

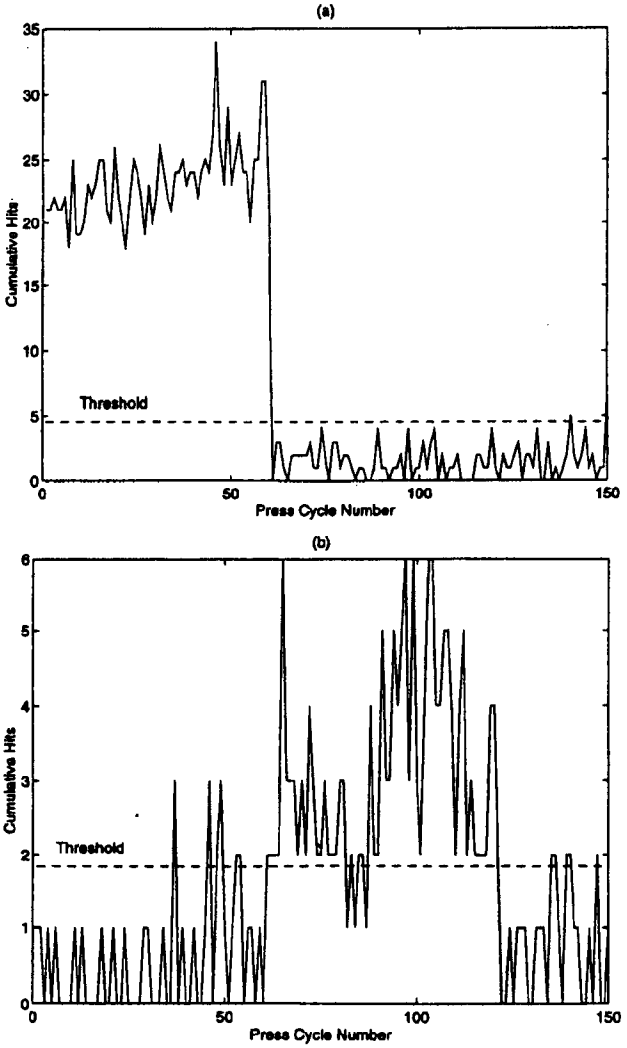

Fig. 6 Cumulative alarms for full sets of Haar coefficients for segments (*a*) S_1 with threshold, $\lambda\sigma_1 = 4.808$, and (*b*) S_2 with threshold, $\lambda\sigma_1 = 1.868$

4. Fault Sensitivity

A counter was used to track the number of times a Haar coefficient exceeded its threshold $\lambda\sigma_i$ (30). The "hits" or number of threshold crossing recorded for each coefficient is shown in Fig. 5. The maximum count of 30 represents a 100 percent hit rate as there were 30 samples for each type of fault. Some coefficients were more sensitive to one type of fault than another. For example, coefficients c_i, $i \in [300 : 350]$, appear to be more sensitive to faults F_1 and F_2 (Fig. 5(*a*), (*b*)) while remaining quite unaffected by faults F_3 and F_4 (Fig. 5(*c*), (*d*)). This is consistent with the fact that highly localized faults affect only Haar coefficients in their support region.

Under no-fault condition, the distribution of hits is quite uniform among all the 512 coefficients (Fig. 5(*e*)). There is no bias in the probability of threshold crossing for any coefficient since the threshold is determined by the variance of each coefficient under normal condition.

5. Detector Output

The cumulative alarms, $\mathcal{A}_j$, $j = 1, 2$ for segments S_1 and S_2 were computed for each press cycle. Figure 6 shows the trajectories of $\mathcal{A}_j$, $j = 1, 2$ over 150 test cycles for the full sets of Haar coefficients C_1 and C_2. The standard deviations for $\mathcal{A}_1$ and $\mathcal{A}_2$ were estimated from the hits registered in Fig. 5(*e*). The thresholds for $\mathcal{A}_1$ and $\mathcal{A}_2$ are respectively 4.808 and 1.868. The detector outputs for S_1 and S_2 are shown in Fig. 7. There were 2 false alarms but no missed detection for S_1 [Fig. 7(*a*)] and 11 false alarms and 3 missed detection for S_2 [Fig. 7(*b*)].

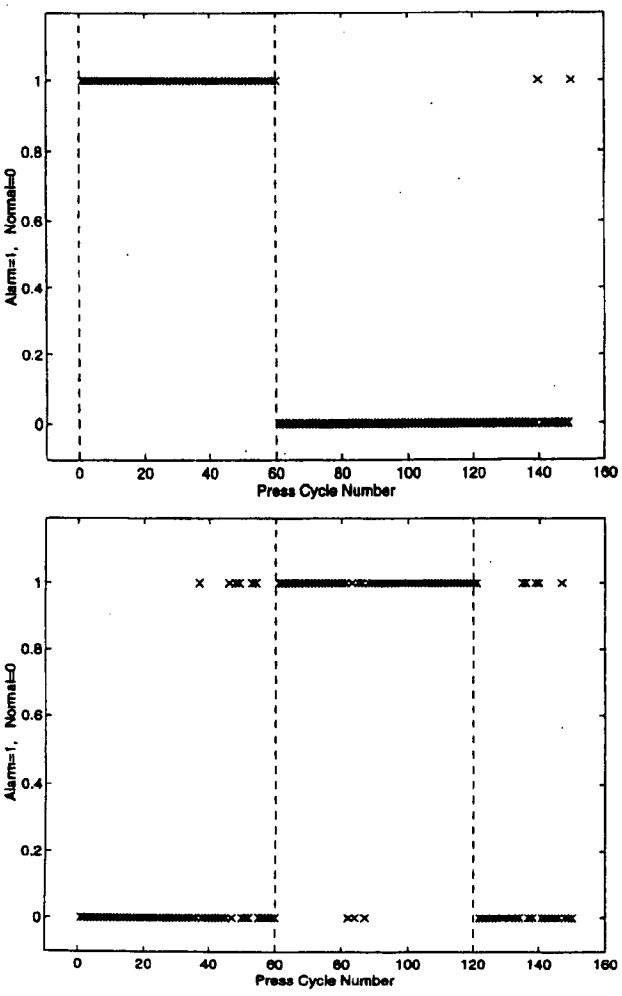

Fig. 7 Output of UMP detector for full sets of Haar coefficients for segments (*a*) S_1 and (*b*) S_2

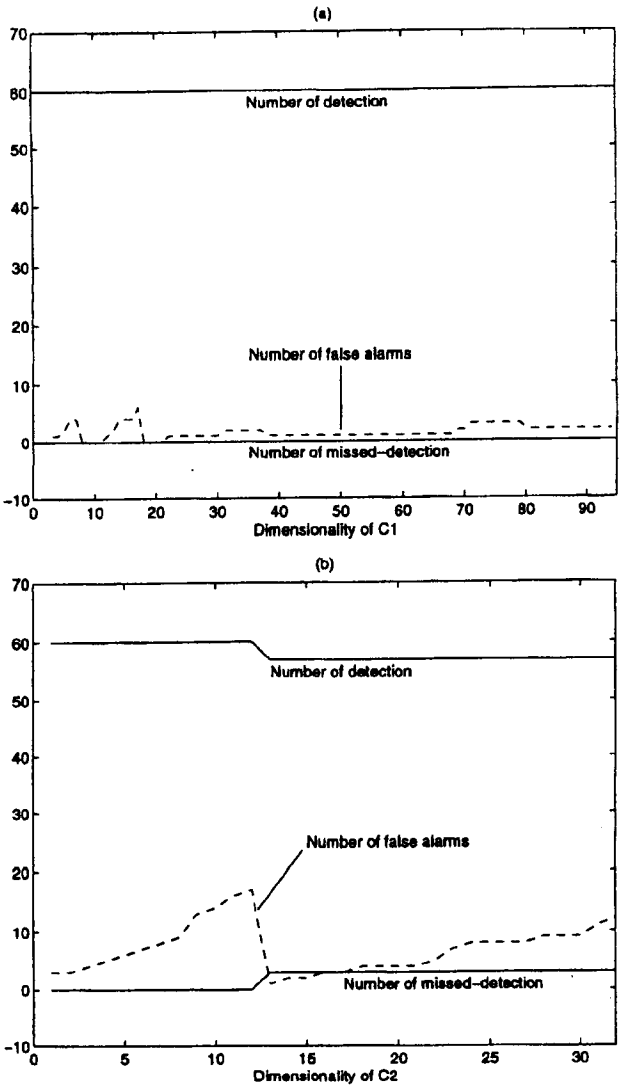

Fig. 8 P_F and P_D as a function of dimension of (*a*) C_1 for S_1 and (*b*) C_2 for S_2

6. Detector Performance

The performance of a Neyman-Pearson detector is completely defined by the values of P_F and P_D. The variation of P_F and P_D as a function of the dimension of C_j is shown in Fig. 8. For example, when the dimension of C_1 is 20 in Fig. 8(*a*), the false alarm rate is zero.

The detector was able to detect the presence of faults F_1 and F_2 in S_1 with any number of coefficients in C_1 [Fig. 8(*a*)]. There is no distinctive trend in the number of false alarms although zero false alarm was possible using just the first two coefficients of C_1.

The detector performance for S_2 dropped slightly when the dimensionality of C_2 exceeded 12 in Fig. 8(*b*). There appears to be two distinct regions of performance. The boundary of the two regions is around the transition in scale of the coefficients in C_2 [Fig. 4(*b*)]. The number of false alarm increases monotonically in both regions. This trend is typical of the "curse of dimensionality" which describes the phenomena of deteriorating performance with increasing number of features used.

The ROC (receiver operating characteristic) curves for segments S_1 and S_2 are shown in Fig. 9. The value of α is derived from [6] for $2.0 \leq \lambda \leq 4.0$. The probability of detection, P_D, defined as the ratio of the number of detection to the number of fault cycles, is 60. The large gap between the cumulative

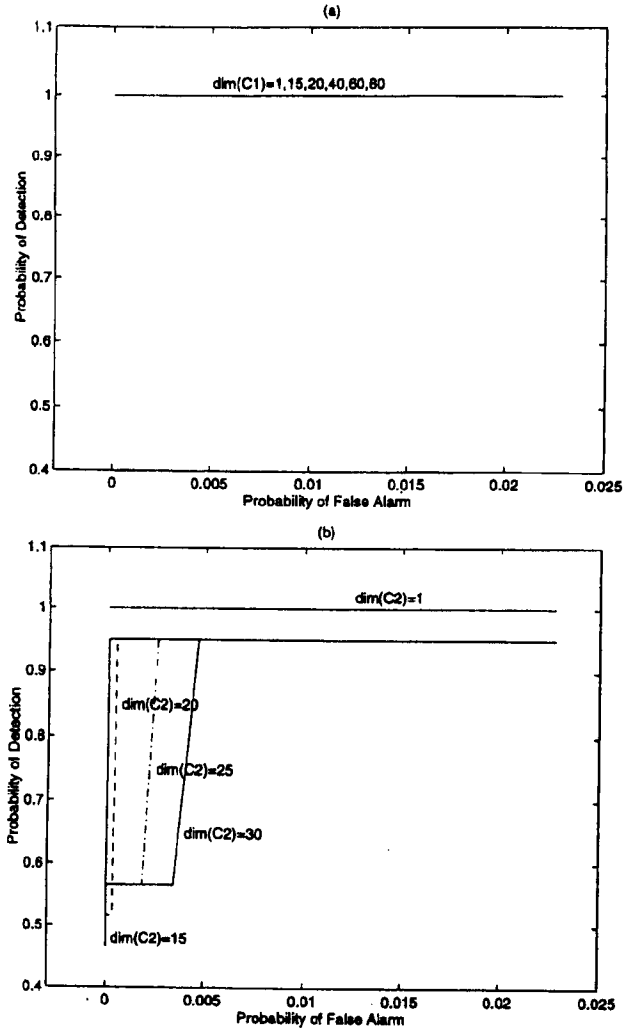

Fig. 9 ROC curves for segments (*a*) S_1 and (*b*) S_2. The horizontal axis shows the probability of false alarm $P_F = \alpha$ corresponding to $2.0 \leq \lambda \leq 4.0$. The vertical axis shows the probability of detection, P_D.

alarms for no-fault and fault conditions in S_1 [Fig. 6(*a*)] explains why the probability of detection, $P_D = 1$ for all dimensionality of C_1. That is, for all $\{c_i\} \in C_1$, $i = 1, 2, \ldots, 94$, $P_D = 1$. The situation is different, however, for S_2 where the cumulative alarms for both conditions are not so well separated [Fig. 6(*b*)]. As the dimensionality of C_2 is increased, the ROC curves indicate a slight deterioration in the detection rate due to the "curse of dimensionality".

An alternative way of presenting the ROC is to plot the actual detection rate, P_D, against the actual false alarm rate, P_F, where

$$P_D = \frac{\text{Number of detections}}{\text{Number of fault cycles}}$$

and

$$P_F = \frac{\text{Number of false alarms}}{\text{Number of normal cycles}}$$

Figure 10 shows such a plot of the ROC curve for segment S_2 for different dimension of C_2. There is a drop in detector performance as the dimension of C_2 increases with more and more higher indexed terms. Eventually, i reaches a value when

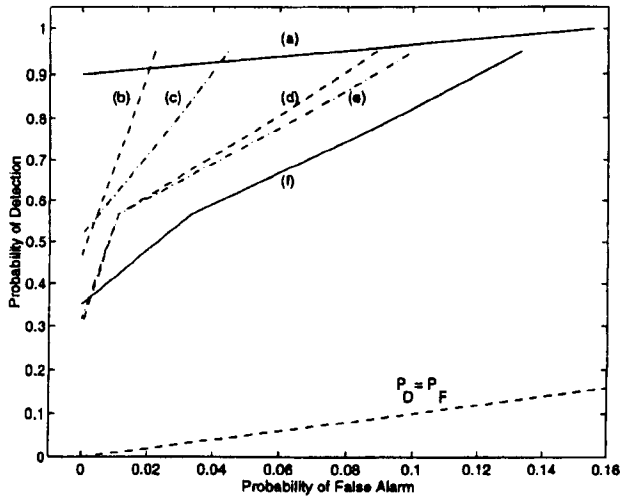

Fig. 10 ROC curves for segment S_2 based on the actual number of detections and false alarms. The corresponding dimensionality of C_2 are (*a*) 10 (*b*) 15 (*c*) 20 (*d*) 25 (*e*) 30 and (*f*) 32.

subsequent coefficients represent only the noise in the data. The performance of the detector is nevertheless superior to that of a randomized test as the ROC curves are all concave downwards and lie above the $P_D = P_F$ line in Fig. 10.

4 Conclusion

The complexity of the stamping process and the number of variables that affect the process pose a very difficult challenge for any kind of on-line fault detection systems. It is an excellent case for the application of detection methodology developed in Part 1. It was shown that Haar coefficients, if properly selected, can perform remarkably well with a UMP detector based on the Neyman-Pearson criteria. The performance of the detector was evaluated with respect to threshold, dimensionality and false alarm rate. This approach can be extended to other manufacturing processes with multiple fault condition.

The authors are grateful to the referees for their helpful comments. The work is partially supported by the NSF Industrial/University Cooperative Research Center at the University of Michigan and Dr. J. Shi was partially supported by NSF CAREER award: DMI 9624402.

References

1 Ahmetoglu, M. A., Altan, T., and Kinzel, G. L., "Improvement of Part Quality in Stamping by Controlling Blank Holder Force and Pressure," *J. Materials Processing Tech.*, Vol. 33, pp. 195–214, 1992.

2 Carabbio, R., "Optimizing Process Control Through Signature Verification," *IPC 93 Technical Symposium.*

3 Clark, A. V., Izworski, N., et al., "Progress Towards Non-destructive, On-line Measurement of Sheet Metal Formability," *Autobody Stamping Technology Progress*, SAE SP-865, Feb. 1991.

4 Koh, C. K-H, Shi, J., and Williams, W. J., "Tonnage Signature Analysis Using the Othogonal Haar Transform," *Transactions of the NAMRC*, pp. 229–234, May 1995.

5 Koh, C. K-H, "Tonnage Signature Analysis for the Stamping Process," PhD Thesis, Univ. of Mich., Aug. 1995.

6 Leon-Garcia, A., *Probability and Random Processes*, Addison Wesley, Table 3.3, pp. 127, 1989.

7 Martinez-Heath, M. R., and Bortfeld, D. P., "Signature Analysis for Machine Control," *Sensors for Manufacturing*, PED-Vol. 26, ASME Winter Annual Meeting, 1987.

8 Near Zero Stamping Inc., "Agile and Precision Sheet Metal Stamping Program," *Technical Report to the National Science and Technology Program*, Advanced Technology Program, 1996.

9 Seem, J. E., and Knussmann, K. D., "Statistical Methods for On-line Fault Detection in Press-working Applications," ASME Winter Annual Meeting, 1994.

10 Siekirt, J. F., "Process Variable Effects on Sheet Metal Quality," *J. of Applied Metalworking*, Vol. 4, No. 3, pp. 262–269, Jul 1986.

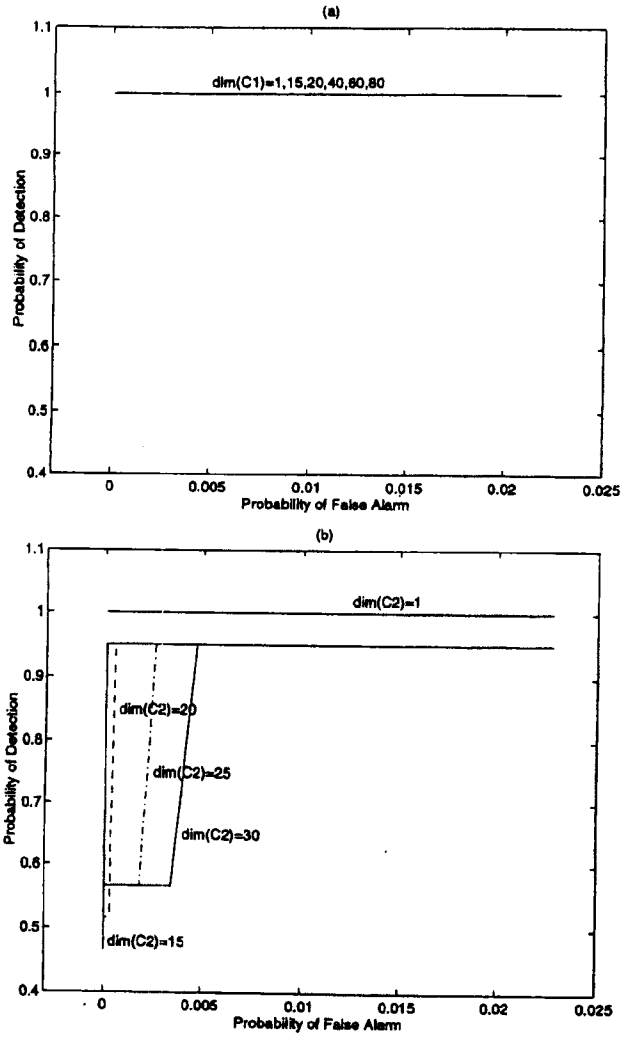

Fig. 9 ROC curves for segments (*a*) S_1 and (*b*) S_2. The horizontal axis shows the probability of false alarm $P_F = \alpha$ corresponding to $2.0 \leq \lambda \leq 4.0$. The vertical axis shows the probability of detection, P_D.

alarms for no-fault and fault conditions in S_1 [Fig. 6(*a*)] explains why the probability of detection, $P_D = 1$ for all dimensionality of C_1. That is, for all $\{c_i\} \in C_1$, $i = 1, 2, \ldots, 94$, $P_D = 1$. The situation is different, however, for S_2 where the cumulative alarms for both conditions are not so well separated [Fig. 6(*b*)]. As the dimensionality of C_2 is increased, the ROC curves indicate a slight deterioration in the detection rate due to the "curse of dimensionality".

An alternative way of presenting the ROC is to plot the actual detection rate, P_D, against the actual false alarm rate, P_F, where

$$P_D = \frac{\text{Number of detections}}{\text{Number of fault cycles}}$$

and

$$P_F = \frac{\text{Number of false alarms}}{\text{Number of normal cycles}}$$

Figure 10 shows such a plot of the ROC curve for segment S_2 for different dimension of C_2. There is a drop in detector performance as the dimension of C_2 increases with more and more higher indexed terms. Eventually, i reaches a value when

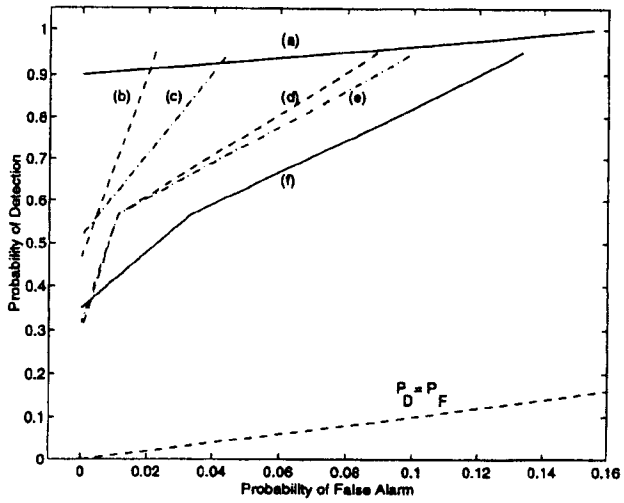

Fig. 10 ROC curves for segment S_2 based on the actual number of detections and false alarms. The corresponding dimensionality of C_2 are (*a*) 10 (*b*) 15 (*c*) 20 (*d*) 25 (*e*) 30 and (*f*) 32.

subsequent coefficients represent only the noise in the data. The performance of the detector is nevertheless superior to that of a randomized test as the ROC curves are all concave downwards and lie above the $P_D = P_F$ line in Fig. 10.

4 Conclusion

The complexity of the stamping process and the number of variables that affect the process pose a very difficult challenge for any kind of on-line fault detection systems. It is an excellent case for the application of detection methodology developed in Part 1. It was shown that Haar coefficients, if properly selected, can perform remarkably well with a UMP detector based on the Neyman-Pearson criteria. The performance of the detector was evaluated with respect to threshold, dimensionality and false alarm rate. This approach can be extended to other manufacturing processes with multiple fault condition.

The authors are grateful to the referees for their helpful comments. The work is partially supported by the NSF Industrial/University Cooperative Research Center at the University of Michigan and Dr. J. Shi was partially supported by NSF CAREER award: DMI 9624402.

References

1 Ahmetoglu, M. A., Altan, T., and Kinzel, G. L., "Improvement of Part Quality in Stamping by Controlling Blank Holder Force and Pressure," *J. Materials Processing Tech.*, Vol. 33, pp. 195–214, 1992.

2 Carabbio, R., "Optimizing Process Control Through Signature Verification," *IPC 93 Technical Symposium.*

3 Clark, A. V., Izworski, N., et al., "Progress Towards Non-destructive, On-line Measurement of Sheet Metal Formability," *Autobody Stamping Technology Progress*, SAE SP-865, Feb. 1991.

4 Koh, C. K-H, Shi, J., and Williams, W. J., "Tonnage Signature Analysis Using the Othogonal Haar Transform," *Transactions of the NAMRC*, pp. 229–234, May 1995.

5 Koh, C. K-H, "Tonnage Signature Analysis for the Stamping Process," PhD Thesis, Univ. of Mich., Aug. 1995.

6 Leon-Garcia, A., *Probability and Random Processes*, Addison Wesley, Table 3.3, pp. 127, 1989.

7 Martinez-Heath, M. R., and Bortfeld, D. P., "Signature Analysis for Machine Control," *Sensors for Manufacturing*, PED-Vol. 26, ASME Winter Annual Meeting, 1987.

8 Near Zero Stamping Inc., "Agile and Precision Sheet Metal Stamping Program," *Technical Report to the National Science and Technology Program*, Advanced Technology Program, 1996.

9 Seem, J. E., and Knussmann, K. D., "Statistical Methods for On-line Fault Detection in Press-working Applications," ASME Winter Annual Meeting, 1994.

10 Siekirt, J. F., "Process Variable Effects on Sheet Metal Quality," *J. of Applied Metalworking*, Vol. 4, No. 3, pp. 262–269, Jul 1986.